Inorganic Chemistry

Article

pubs.acs.org/IC

Hydrothermal Crystal Growth and Structure Determination of Double Hydroxides $LiSb(OH)_6$, $BaSn(OH)_6$, and $SrSn(OH)_6$

Hiroshi Mizoguchi,[†] Nattamai S. P. Bhuvanesh,[‡] Young-Il Kim,[§] Satoshi Ohara,[∥] and Patrick M. Woodward*[,⊥]

[†]Frontier Research Center, Tokyo Institute of Technology, Yokohama 226-8503, Japan

[‡]Department of Chemistry, Texas A&M University, College Station, Texas 77842-3012, United States

[§]Department of Chemistry, Yeungnam University, Gyeongsan 712-749, Republic of Korea

[∥]Joining & Welding Research Institute, Osaka University, 11-1, Mihogaoka, Ibaraki, Osaka 567-0047, Japan

[⊥]Department of Chemistry and Biochemistry, The Ohio State University, Columbus, Ohio 43210-1185, United States

Supporting Information

ABSTRACT: Colorless single crystals of $LiSb(OH)_6$, $SrSn(OH)_6$, and $BaSn(OH)_6$, which are useful as precursors for the synthesis of $LiSbO_3$, $SrSnO_3$, and $BaSnO_3$, were synthesized by a low-temperature hydrothermal method using a Teflon-lined autoclave at 380 K. The crystal structures were determined by single-crystal X-ray diffraction measurements. $LiSb(OH)_6$ crystallizes in the trigonal space group $P\bar{3}1m$ with a = 5.3812(3)A, c = 9.8195(7)A, V = 246.25(3)A^3, Z = 2. In this layered structure, $[Li_2Sb(OH)_6]^+$ and $[Sb(OH)_6]^-$ layers are alternately stacked along the c-direction. The $[Li_2Sb(OH)_6]^+$ layer can be regarded as a cation-ordered $CdCl_2$ layer. The $[Sb(OH_6)]^-$ layer is built up from isolated $[Sb(OH)_6]^-$ octahedra, which are linked to each other via hydrogen bonding within the layer. $BaSn(OH)_6$ and $SrSn(OH)_6$ crystallize with monoclinic $P2_1/n$ space group symmetry. The monoclinic structure possesses a CsCl-type packing of Ba^{2+}/Sr^{2+} cations and $[Sn(OH)_6]^{2-}$ anions. The $[Sn(OH)_6]^{2-}$ polyhedra are connected to each other through hydrogen bonding to form a three-dimensional framework. The factors that favor these hitherto unknown crystal structures are discussed using a structure map that compares various $M(OH)_3$ and $M'M''(OH)_6$ compounds.

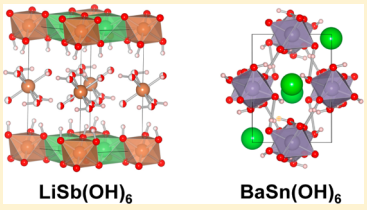

INTRODUCTION

Complex hydroxides have long been known as effective intermediate phases for preparing oxides of interest.[1] In particular, the double hydroxides $M'^{2+}M''^{4+}(OH)_6$ or $M'^{+}M''^{5+}(OH)_6$ are potential precursors for preparing $M'M''O_3$ perovskite oxides. Given the significance of perovskite phases both in fundamental and applied areas of solid-state chemistry, it is of interest to examine the formation and structure of $M'M''(OH)_6$-type compounds. In this work, we consider three double hydroxides, $LiSb(OH)_6$, $SrSn(OH)_6$, and $BaSn(OH)_6$, which can act as precursors for the synthesis of the ternary oxides $LiSbO_3$, $SrSnO_3$, and $BaSnO_3$, respectively.

The stannate perovskites, $BaSnO_3$ and $SrSnO_3$, are of interest for a variety of reasons. Recently, a large electrical conductivity of ~10^4 S/cm was reported on epitaxial film of $BaSnO_3$.[2] This observation coupled with its band gap of 3.1 eV makes it a promising candidate for use as a transparent conductive oxide.[3] In addition, $BaSnO_3$ exhibits strong near-infrared luminescence at room temperature.[4] $SrSnO_3$ has attracted attention recently as the anode material for lithium ion batteries and as a phosphor host for blue emission.[5] The hydroxides $M'Sn(OH)_6$ (M' = Sr and Ba) have been successfully utilized for low-temperature synthesis of $BaSnO_3$ and $SrSnO_3$ via thermal decomposition,[4,6] but the crystal structures of these hydroxides have yet to be elucidated. $M'Sn(OH)_6$ compositions (M' = Mg, Ca, Mn, Fe, Zn, Cd) exclusively adopt the rock salt (RS)-ordered ReO_3 structure,[7,8] and it is interesting to see whether the same trend is maintained for the bigger M' ions such as Sr^{2+} and Ba^{2+}.

$LiSb(OH)_6$ is considered as a precursor for the preparations of $LiSbO_3$ and protonated $HSbO_3{\cdot}nH_2O$.[9] While a hexagonal unit cell (a = 5.351 Å, c = 4.918 Å) of $LiSb(OH)_6$ was reported in 1938 by Schrewelius,[10] no further details have been revealed until now. In this paper, we report the low-temperature hydrothermal synthesis of single crystals of $LiSb(OH)_6$ and $M'Sn(OH)_6$ (M' = Sr and Ba) and their structures as determined by single-crystal X-ray diffraction (XRD). The single crystal X-ray diffraction method proved essential for the present study, especially for the structure determination of $LiSb(OH)_6$ containing the weakly scattering Li^+ and H^+. These structures are then compared to the crystal structures of a wide variety of $M(OH)_3$ and $M'M''(OH)_6$ hydroxides to better understand the bonding interactions that determine the crystal structures of metal hydroxides.

EXPERIMENTAL SECTION

Hydrothermal conditions were used for the low-temperature synthesis of $LiSb(OH)_6$ and $M'Sn(OH)_6$ (M' = Sr or Ba). For the synthesis of $LiSb(OH)_6$, source materials, namely, $LiOH{\cdot}H_2O$ (99.95%, Aldrich,

Received: July 14, 2014
Published: September 10, 2014

   dx.doi.org/10.1021/ic5016252 | Inorg. Chem. 2014, 53, 10570−10577

Table 1. Structure Refinement Details from Single-Crystal X-ray Diffraction

empirical formula	$LiSb(OH)_6$	$BaSn(OH)_6$	$SrSn(OH)_6$
temp (K)	298	293	293
wavelength (Å)	0.710 73	0.710 73	0.710 73
crystal system	trigonal	monoclinic	monoclinic
space group	$P\bar{3}1m$	$P2_1/n$	$P2_1/n$
Z	2	4	4
fw	230.74	358.08	308.36
unit cell dimensions	a = 5.3812(3) Å	a = 9.3928(2) Å	a = 9.5306(4) Å
	c = 9.8195(7) Å	b = 6.3440(1) Å	b = 6.0105(2) Å
		c = 10.5679(2) Å	c = 10.2610(4) Å
		β = 113.205(1)°	β = 113.301(2)°
V (Å^3)	246.25(3)	578.78(2)	539.85(4)
density (calculated) (g cm^{-3})	3.112	4.109	3.794
μ (mm^{-1})	5.540	11.029	14.455
F(000)	216	640	568
cryst size (mm)	0.20 × 0.19 × 0.05	0.08 × 0.12 × 0.19	0.20 × 0.10 × 0.10
θ max (deg)	29.86	27.49	27.45
no. of reflns collected	2164	17 297	5046
no. of independent reflns	262	1329	1234
goodness-of-fit on F^2	1.173	1.158	1.095
min/max transmission	0.4073/0.7692	0.334/0.414	0.1952/0.7357
$R(F)$	0.0243	0.0148	0.0297
$R_w(F^2)$	0.0271	0.0202	0.0586
largest diff. peak/hole (e Å^{-3})	0.671 and −0.743	1.383 and −0.602	1.432 and −1.135

Table 2. Atomic Coordinates and Displacement Factors for $LiSb(OH)_6$

	Wyckoff	x	y	z	U(eq) (Å × 10^3)[a]
Li	2c	1/3	2/3	0	13(2)
Sb(1)	1b	0	0	1/2	13(1)
Sb(2)	1a	0	0	0	9(1)
O(1)[b]	12l	0.150(1)	0.343(1)	0.3818(4)	19(1)
O(2)	6k	0.3093(6)	0	0.1068(2)	12(1)
H	6k	0.37(1)	0	0.621(6)	3(2)

[a] U(eq) is defined as one-third of the trace of the orthogonalized U^{ij} tensor. [b] The occupancy factor for O(1) is 0.5.

2.8 mmol) and $KSb(OH)_6$ (99.99%, Aldrich, 2.3 mmol), were placed with water (10 mL) in a Teflon-lined autoclave, and kept at 383 K for 1 d. For the synthesis of $M'Sn(OH)_6$ (M′ = Sr or Ba), source materials, namely, $M'Cl_2{\cdot}2H_2O$ (M′ = Sr or Ba, 99.95%, Mallinckrodt, 0.15 mmol) and $K_2Sn(OH)_6$ (99.9%, Aldrich, 0.13 mmol), were placed with water (10 mL) in a Teflon-lined autoclave, and kept at 373 K for 1 d. Small colorless single crystals were obtained. They were collected by filtration, washed twice with water and once with acetone, and then dried at 323 K in air.

Isolated crystals were identified as $LiSb(OH)_6$ and $M'Sn(OH)_6$ (M′ = Sr and Ba) from the powder XRD method. Infrared (IR) spectra with the samples dispersed in KBr pellets were collected on a PerkinElmer 1600 IR spectrometer. Thermogravimetry (TG) and differential thermal analysis (DTA) were conducted with a RIGAKU TAS-200 instrument under air with alumina powder as a reference. Powder XRD data suitable for structure refinement were collected at 300 K with Debye−Scherrer optics (Bruker D8, anode: sealed Cu X-ray tube with 40 kV and 50 mA) equipped with an incident beam Ge 111 monochromator, which passes Cu Kα1 radiation only (λ = 1.5406 Å). The pulverized single crystals were sealed in a glass capillary with a diameter of 0.2 mm. The capillary was rotated continuously about its long axis during data collection to average out the preferential orientation effect. Synchrotron XRD pattern was also collected with Debye−Scherrer optics at the beamline X7A of the National Synchrotron Light Source (Brookhaven National Laboratory) using the X-ray radiation of λ = 0.8051 Å. Structure refinements were performed by the Rietveld method using the TOPAS software package.[11]

Single-crystal XRD data were collected on a Bruker SMART APEX CCD system at room temperature using graphite-monochromated Mo Kα radiation (λ = 0.710 73 Å). The Bruker SAINTplus program was used for integration.[12] Absorption correction was applied by SADABS.[12] The crystal structure was solved by direct methods and refined with the full matrix least-squares method on F^2. All calculations were performed using the Bruker SHELXTL package.[13] Further details for data collection and the crystal data are given in Tables 1−5, in Supporting Information, Tables S1−S3, and in available CIF files. The bond valence sums (BVS) were calculated with the aid of the program VALENCE,[14] using the bond valence parameters R_0(Li−O) = 1.466 Å, R_0(Sb−O) = 1.942 Å, R_0(H−O) = 0.882 Å, and R_0(Sn−O) = 1.905 Å.

Table 3. Selected Bond Distances (Å) for $LiSb(OH)_6$

Sb(1)−O distances (Å)	Sb(2)−O distances (Å)	Li−O distances (Å)
O(1) 1.978(5) × 6[a]	O(2) 1.968(3) × 6	O(2) 2.137(2) × 6

[a] Since O(1) locates on 12l site with occupancy factor of 0.5, each Sb(1) atom is locally coordinated by six O(1) atoms.

RESULTS

$LiSb(OH)_6$. The colorless transparent single crystals with hexagonal shape were piled up on each other, as shown in the SEM image of Figure 1a. Obtained single crystals were pulverized for TG and DTA measurements. Supporting

dx.doi.org/10.1021/ic5016252 | Inorg. Chem. 2014, 53, 10570−10577

Table 4. Selected Bond Distances (Å) for M′Sn(OH)$_6$ (M′ = Sr and Ba)

	Sn(1)−O distances (Å)	Sn(2)−O distances (Å)	M′−O distances (Å)
BaSn(OH)$_6$	O(1) 2.046(2) × 2	O(6) 2.030(2) × 2	2.714(2), 2.746(2),
	O(5) 2.055(2) × 2	O(4) 2.073(2) × 2	2.758(2), 2.773(2),
	O(2) 2.060(2) × 2	O(1) 2.093(2) × 2	2.786(2), 2.800(2),
			2.844(2), 3.104(2)
SrSn(OH)$_6$	O(1) 2.037(3) × 2	O(6) 2.032(3) × 2	2.554(3), 2.560(3),
	O(5) 2.074(3) × 2	O(4) 2.056(3) × 2	2.571(3), 2.588(3),
	O(2) 2.092(3) × 2	O(1) 2.060(3) × 2	2.603(3), 2.665(3),
			2.670(3), 3.375(4)

Table 5. Hydrogen Bonds in BaSn(OH)$_6$

hydrogen bond	*D*−H (Å)	H···*A* (Å)	*D*···*A* (Å)	∠(*DHA*) (deg)
O(1)−H(1)···O(3)	0.947	2.494	3.085(3)	120.5
O(1)−H(1)···O(1)	0.947	2.521	3.446(2)	165.4
O(2)−H(2)···O(4)	0.894	2.002	2.895(3)	176.8
O(3)−H(3)···O(1)	1.034	1.889	2.906(3)	167.1
O(4)−H(4)···O(3)	0.902	2.755	3.375(3)	126.9
O(5)−H(5)···O(6)	0.946	1.881	2.821(3)	172.3
O(6)−H(6)···O(3)	0.983	1.755	2.737(3)	178.2

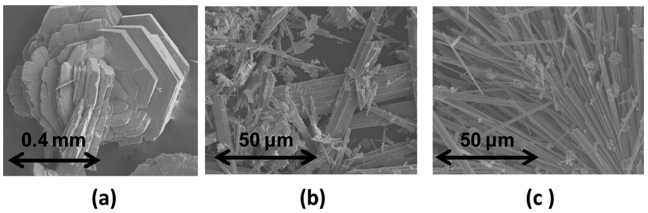

Figure 1. SEM images of (a) platelike single crystals of LiSb(OH)$_6$ which are piled on top of each other, and needlelike crystals of (b) BaSn(OH)$_6$ and (c) SrSn(OH)$_6$. The SrSn(OH)$_6$ crystals were synthesized without the use of H_2O_2.

Information, Figure S1a shows the endothermic decomposition of the hydroxide near 210 °C, accompanied by weight loss of ~24%. Powder XRD measurement indicated the formation of $LiSbO_3$ at the completion of TG, as reported in the literature.[9] Taking the evolution of gaseous H_2O into consideration, the sample was identified as LiSb(OH)$_6$ with no additional water molecules.

As shown in Figure 2, the IR spectra of pulverized single crystals agreed well with the reported spectra of polycrystalline samples.[9] Sharp peaks due to OH stretching, which can be assigned to particular H sites, were not detected, except for a weak shoulder around 3210 cm^{-1}.

Crystals with a suitable size were cleaved and used for single crystal XRD measurements. The structure was solved in the centrosymmetric space group, $P\bar{3}$ with a hexagonal unit cell of a = 5.3812(3) Å and c = 9.8195(7) Å. Additional symmetries were found by the program ADDSYM in the PLATON suite of programs,[15] and the structure was transformed into the space group, $P\bar{3}1m$. The light atoms Li and H were located from difference Fourier maps, and a common isotropic displacement parameter was used for H atoms (Table 2). It was possible to determine only half of the H positions, due in part to the presence of heavy and strongly diffracting Sb neighbors. There were a few crystals that showed superstructure diffraction spots originating from a $4a \times 4a \times c$ superlattice, but we were not able to get a valid structure solution of the cell. No superstructure reflections were found in the powder XRD pattern (Figure 3). Rietveld refinements yield practically the

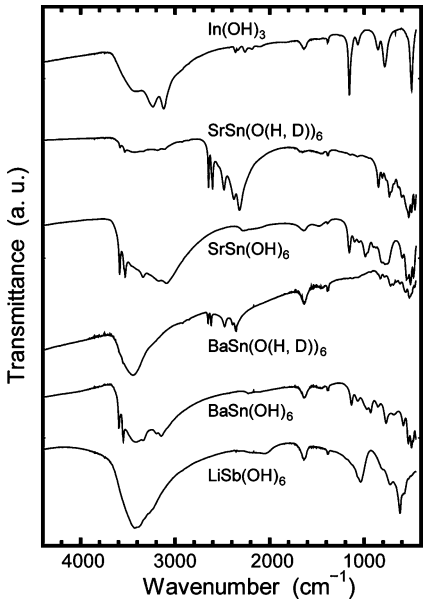

Figure 2. Infrared transmission spectra of In(OH)$_3$, M′Sn(OH)$_6$ (M′ = Sr, Ba), and LiSb(OH)$_6$ collected in transmission mode by dispersing the samples in KBr pellets. To clarify the region of OH stretching mode, samples synthesized in D_2O were also measured.

same structural parameters as those obtained by the single-crystal structure analysis, indicating negligible preferred orientation effects.

The structure of LiSb(OH)$_6$ is shown in Figure 4a, and select bond distances are given in Table 3. In this hitherto unknown structure, [Li$_2$Sb(OH)$_6$]$^+$ and [Sb(OH)$_6$]$^-$ layers are alternately stacked along the c axis. The detail of each layer is shown in Figure 4b,c. The Sb(1) and Sb(2) atoms occupy 1*b* and 1*a* sites with D_3 site-symmetry, respectively, and reside on the S_3 axis. Both Sb ion types are octahedrally coordinated by O^{2-} (OH^-) ions. The bond valence sums of Sb(1) and Sb(2) are 5.44 valence unit (vu) and 5.59 vu, respectively, indicating moderately short Sb−O distances. Li occupies a 2*c* site with D_{3d} site-symmetry, and is located on the C_3 rotation axis. Li also takes octahedral coordination, and has a bond valence sum of

dx.doi.org/10.1021/ic5016252 | Inorg. Chem. 2014, 53, 10570−10577

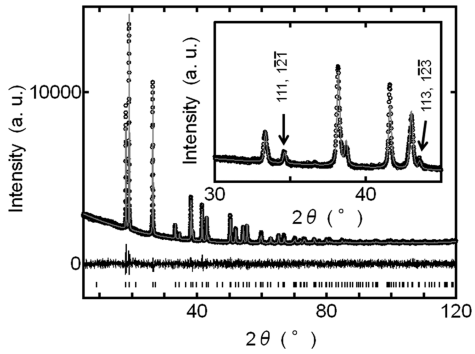

Figure 3. Observed powder X-ray diffraction pattern for $LiSb(OH)_6$ along with calculated and difference patterns from the Rietveld refinement of its structure. The vertical tick marks indicate the expected 2θ position of the reflections. Obtained structural parameters agreed with those in Table 2, although the Li and H positions could not be accurately determined from X-ray powder data. (inset) An enlargement of the 2θ region from 30 to 45° showing the several reflections with odd values of l confirming the c-axis length of ~9.82 Å.

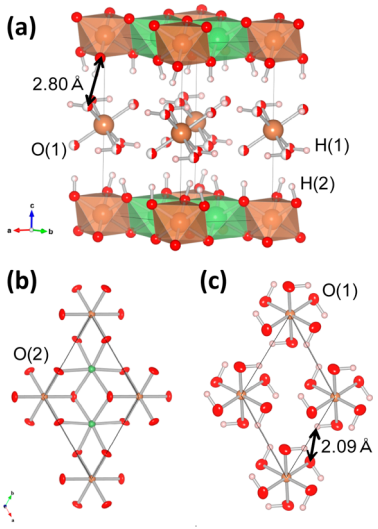

Figure 4. (a) The crystal structure of $LiSb(OH)_6$. Li^+ and Sb^{5+} are shown as green and brown spheres, respectively, while O^{2-} and H^+ are shown as red and pink spheres, respectively. A split site model with an occupancy of 0.5 was used for the O(1) and H(2) sites. For clarity, only one-half of the occupied O(1) and H(2) sites are shown. The position of H(2) in the interlayer (12l site, (~0.26, ~0.94, ~0.20) with occupancy factor of 0.5) was estimated on the basis of bond valence calculations. (b) The $[Li_2Sb(OH)_6]^+$ and (c) $[Sb(OH)_6]^-$ layers seen in $LiSb(OH)_6$. The ellipsoids represent 85% of their probability.

0.98 vu. Both Li and Sb(2) atoms are located on the z = 0 plane, forming the $CdCl_2$-like slabs with composition $[Li_2Sb(OH)_6]^+$.

Within the $[Sb(OH)_6]^-$ layer, the $Sb(OH)_6$ octahedra are isolated from each other, but are interconnected via hydrogen bonds. The features of the hydrogen bond in this layer are shown in Supporting Information, Table S1. The Sb(1)-centered octahedra that make up this layer can take on two different orientations, resulting in the half-occupation of the 12l site by O(1) atom. The appearance of superstructure reflections within the ab plane may be related with medium-range orientational ordering of the isolated $[Sb(OH)_6]^-$ octahedra.

Next, we examine the interlayer connection between $[Li_2Sb(OH)_6]^+$ and $[Sb(OH)_6]^-$ layers. The O(1)−O(2) distance (2.80 Å) is similar to that of $In(OH)_3$ (2.73 Å),[16] indicating the existence of a medium-strength hydrogen bond in the interlayer space. The missing hydrogen atom H(2) is likely to reside between the layers and contribute to the link between them. The position of H(2) atoms was estimated using bond valence calculations to be approximately (~0.26, ~0.94, ~0.20) on the 12l site with an occupancy factor of 0.5, as represented in Figure 4a. The fractional occupancy of the H(2) atoms is presumably one of the factors that complicate the single-crystal XRD analysis.

Lithium ions reside in every other $Sb(OH)_6$ layer along the c-direction, as indicated by the diffraction peaks whose Miller Indices hkl have an odd value of l. In the absence of Li the two layers would be identical, but the ordering of Li into every other layer doubles the length of the c-axis to a value of roughly 9.82 Å. The intensities of the reflections where $l = 2n + 1$ are relatively weak and easy to overlook. Indeed, Schrewelius reported a hexagonal unit cell (a = 5.351 Å and c = 4.918 Å) for $LiSb(OH)_6$ in 1938 on the basis of powder XRD measurements.[10] However, as shown in the inset of Figure 3, the 111, 12̄1, 113, and 12̄3 diffraction peaks are clearly observable, confirming the doubling of the c-axis.

M′Sn(OH)$_6$ (M′ = Sr or Ba). Needle-shaped crystals of $M'Sn(OH)_6$ (M′ = Sr or Ba) were obtained by the hydrothermal process, as shown in Figure 1 (b) and (c). The $SrSn(OH)_6$ crystals were too small for single crystal structure analysis, when prepared from $SrCl_2{\cdot}2H_2O$ and $K_2Sn(OH)_6$ only. However, larger crystals, several mm long, could be synthesized by adding H_2O_2 (~1 mL) to the autoclave. The cation ratio was estimated to be Ba/Sn ≈ Sr/Sn ≈ 1, using EDS. Via powder XRD measurements, crystals were identified to be $M'Sn(OH)_6$ and their powder diffraction patterns matched those reported in PDF (JCPDS) database.[17] We hypothesize that hydroxides form under these conditions because the low-temperature synthesis ($T \approx$ 373 K) suppresses dehydration. According to the TG and DTA measurements shown in Supporting Information, Figure S1b $BaSn(OH)_6$ decomposes in two dehydration steps, at 250 and 340 °C, and crystallizes as $BaSnO_3$ at 600 °C. The total observed weight loss, 13.5%, indicates that no crystalline water existed in this compound. On the other hand, TG measurements indicate that the as-prepared $SrSn(OH)_6$ crystals do contain additional water, with a composition of $SrSn(OH)_6{\cdot}0.93H_2O$. According to the diffraction analysis described below the additional water was not crystalline.

The structures of $M'Sn(OH)_6$ are shown in Figure 5 and select bond distances and characteristics of hydrogen bond are given in Tables 4 and 5, respectively. Additional details can be found in Supporting Information, Tables S2 and S3. These isostructural compounds crystallize with monoclinic $P2_1/n$ space group symmetry. For both compounds, experimental powder XRD patterns agreed well with the simulated one based on single-crystal structure analysis (Supporting Information, Figure S2), indicating the validity of the obtained crystal structure. The oscillation image collected by X-ray rotation camera showed that the period of the rotation axis, that is, the long axis of the needle-shaped crystal, agreed well with the length of the b-axis of the unit cell.

In the crystal structure of $BaSn(OH)_6$ the Sn(1) and Sn(2) atoms occupy the 2c and 2d sites, respectively, which are the inversion centers with C_i site-symmetry. The tin is octahedrally coordinated with Sn−O distances (Table 4) very close to those reported for related compounds, such as $CaSn(OH)_6$.[18] The

dx.doi.org/10.1021/ic5016252 | Inorg. Chem. 2014, 53, 10570−10577

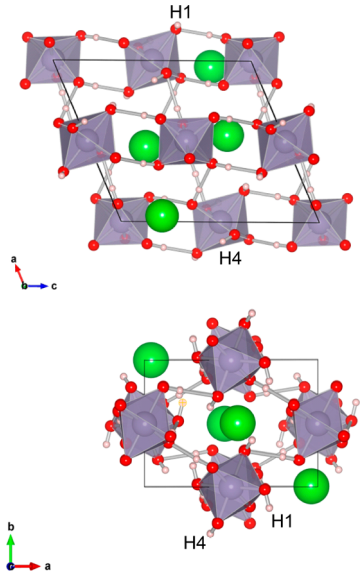

Figure 5. Crystal structure of $BaSn(OH)_6$. Ba^{2+} and Sn^{4+} are shown as green and violet spheres, respectively, while the O^{2-} and H^+ are shown as red and pink spheres, respectively.

calculated BVS values are 4.01 and 3.90 vu for Sn(1) and Sn(2), respectively, indicating the Sn^{4+} valence state. All other atoms are located at the 4*e* sites. There are six O sites, O(1) through O(6), each of which is coordinated by an H atom. The $Sn(OH)_6$ polyhedra are isolated and adopt a distorted simple cubic structure, and the body-centered cavity is filled with a Ba^{2+} ion. In other words, the structure adopts a distorted CsCl arrangement of Ba^{2+} cations and $[Sn(OH)_6]^{2-}$ anions. The large Ba ion is coordinated by eight O ions, and the Ba–O distances range from 2.71 to 3.10 Å, with the average distance of 2.816 Å (Table 4). Note that the cations in a perovskite lattice possess a CsCl arrangement, which suggests an easy conversion from the $BaSn(OH)_6$ into $BaSnO_3$ via thermal decomposition.

As seen in Figure 5, the isolated $Sn(OH)_6$ polyhedra connect to each other along *c*-axis via hydrogen bonds involving H(3) and H(5) (D···A distances: 2.91, 2.82 Å), while we see hydrogen bonds along the [110] and [1$\bar{1}$0] directions via H(2) and H(6), respectively (D···A distances: 2.90, 2.74 Å), resulting in the formation of a three-dimensional (3D) simple cubic framework of $[Sn(OH)_6]^{2-}$ octahedra connected by relatively modest strength hydrogen bonds. While all the H atoms of $[Sn(1)(OH)_6]^{2-}$ polyhedron contribute to the hydrogen bond network, only two of the hydroxide ions in the $[Sn(2)(OH)_6]^{2-}$ polyhedron take part in hydrogen bonding. As seen in Figure 5 and Table 5, the remaining sites, H(1) and H(4), do not form hydrogen bonds. Although the observed pattern of hydrogen bonding suggests a stronger chemical bond along *c*-axis, the long axis of the needle-shaped crystal was the *b*-axis, as observed in the rotation photograph.

The information obtained from the IR spectra is often useful for estimating the strength of a hydrogen bond. To emphasize the spectral components associated with the hydrogen bonds, the spectra were also collected on the samples synthesized in D_2O. As shown in Figure 2, we often see the absorption band due to the bending mode of adsorbed water near ~1600 cm^{-1}. Five to six bands of the OH stretching mode in $M'Sn(OH)_6$ were observed in the region of 3100–3700 cm^{-1} and were ascribed to each H site, while the 3–4 bands were found near 3100–3420 cm^{-1} in $BaSn(OH)_6$ and correspond to moderate strength hydrogen bonds. Two sharp bands near 3500–3600 cm^{-1} in the spectra of both $BaSn(OH)_6$ and $SrSn(OH)_6$ are ascribed to the H(1) and H(4) atoms, which do not form hydrogen bonds and are therefore more tightly bound to a single O atom.

DISCUSSION

It is instructive to compare the structures of these three compounds with those of other hydroxides with a similar stoichiometry. The crystal structures of known $M(OH)_3$ and $M'M''(OH)_6$ compounds, including those of the present study, are summarized in a structure map based on the ionic radii of the M′ and M″ cations shown in Figure 6. The effective separation of the different structure types shows that the structures of these hydroxides are dictated by the size and electronegativity of the cation(s).

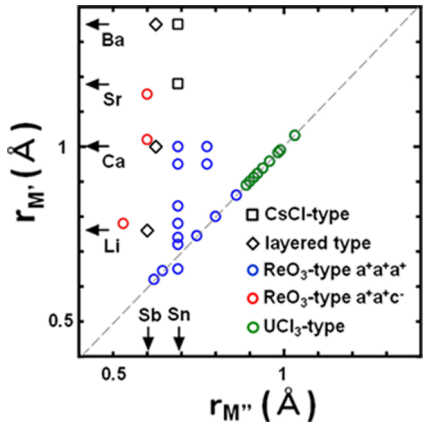

Figure 6. Structure map of ReO_3-type related hydroxides including $M(OH)_3$ and $M'M''(OH)_6$. The ionic radii for octahedral coordination reported by Shannon[19] were used to construct the plot.

The trihydroxides of electropositive and larger cations (Y, La, Pr, Nd, Sm, Gd, Tb, Dy, Er, and Yb) crystallize in the UCl_3 structure.[8] In this hexagonal structure the M^{3+} cation is surrounded by nine OH^- ions and each OH^- by three M^{3+} ions. The preference for this structure type is presumably driven by the larger size of the cation, which favors higher coordination number, and the reduced electronegativity of the cation, which favors enhanced ionic interactions.

The binary hydroxides containing trivalent cations of intermediate electronegativity and smaller radii (Sc, Fe, Ga, In, and Lu) crystallize with the ReO_3-type structure.[7,8] This structure consists of a 3D framework of corner-shared octahedra, as shown in Figure 7a. While the aristotype ReO_3 structure is cubic with linear Re–O–Re bonds, in these hydroxides the structure is distorted by tilting of the metal-centered octahedra driven by the attractive interaction between the O atoms through hydrogen bonds. This kind of tilting is similarly observed in skutterudite $CoAs_3$ with an anion–anion bond,[7] and is represented by the Glazer notation $a^+a^+a^+$.[20]

$In(OH)_3$ is a representative example of the ReO_3-type hydroxides with $a^+a^+a^+$ tilting.[16] The structure of $In(OH)_3$ is distorted from the ideal $Pm\bar{3}m$ symmetry by in-phase rotations of the octahedra (Figure 7a). The octahedral tilting in $In(OH)_3$ is driven at least in part by the formation of hydrogen bonds between neighboring octahedra. In this highly symmetric structure every hydrogen atom forms hydrogen bonds with

dx.doi.org/10.1021/ic5016252 | *Inorg. Chem.* 2014, 53, 10570–10577

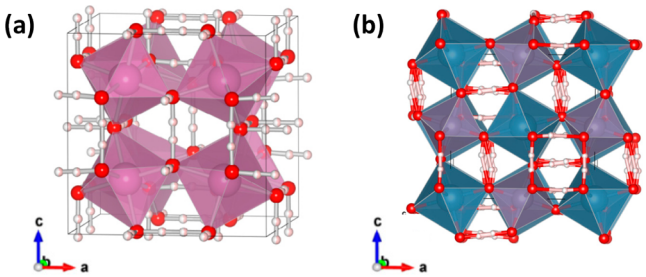

Figure 7. Crystal structures of (a) $In(OH)_3$ ($Im\bar{3}$, a = 7.974 Å),[16] and (b) $CaSn(OH)_6$ ($Pn\bar{3}$, a = 8.135 Å),[18] Ca^{2+}, In^{3+}, Sn^{4+}, and O^{2-} are shown as blue, purple, violet, and red spheres, respectively. The hydrogen atoms are shown as white spheres, and only one of two neighboring white spheres are occupied (a split site model).

an oxygen atom of a neighboring octahedron. Bending the In−O−In bonds that would be linear in the undistorted $Pm\bar{3}m$ structure serves another purpose as well. It allows for more favorable participation of the oxygen 2p orbitals in bonding with indium. This effect has been discussed in the context of the preferred structures of compounds such as TeO_3, which has the ReO_3 structure with highly bent Te−O−Te bonds.[21]

Moving onto the ternary perovskites an ReO_3-type structure is preferred by most of the $M'M''(OH)_6$ compounds. For example, all of the $M'Sn(OH)_6$ (M' = Mg, Ca, Mn, Co, Zn, Cd) compounds have the ReO_3-structure with RS-type ordering of the M' and Sn^{4+} ions and $a^+a^+a^+$ tilting of the octahedra, as shown in Figure 7b.[7,8] The ternary hydroxides $NaSb(OH)_6$, $AgSb(OH)_6$, and $FeGe(OH)_6$ also adopt an RS-ordered ReO_3-type structure, but interestingly these structures take a different pattern of octahedral tilting, $a^+a^+c^-$.[7,22]

It is interesting to consider the tilt patterns seen in ReO_3-type hydroxides more closely. Lufaso and Woodward have compiled the distribution of the tilt systems among known perovskites with a single octahedral cation and have shown that the $a^-b^+a^-$, $a^-a^-a^-$ and $a^+a^+a^+$ tilting modes are the most common.[23] While these three tilting schemes are equally effective in bending the M−X−M bonds they have different consequences for the size and shape of the cavities between octahedra (where the A cations reside in a perovskite) as well as the anion−anion distances.

While $a^-b^+a^-$ is the most common in perovskites for reasons that have been explained elsewhere,[20] the other two tilt systems are dominant in compounds with the ReO_3-type structure. Among MF_3 compounds $a^-a^-a^-$ tilting dominates, because it maximizes the interoctahedral anion−anion distances, and thereby has the most favorable lattice energy.[20] Conversely, the $M(OH)_3$ hydroxides show $a^+a^+a^+$ tilting exclusively, as do $M'Sn(OH)_6$ (M' = Mg, Ca, Zn, or Cd) compounds. As discussed earlier this pattern of octahedral tilting appears to be optimal for maximizing the hydrogen bonding interactions. As the size and electronegativity difference between M' and M'' ions increases the $a^+a^+c^-$ tilting mode appears. This tilting mode is exceedingly rare in perovskites as well as oxides or halides with ReO_3-type structures, which suggests that its appearance in hydroxides is likely related in some way to hydrogen-bonding interactions. In fact, Ross et al. have shown that in $FeGe(OH)_6$, which exhibits $a^+a^+c^-$ tilting, the hydrogen-bonding interactions are confined to (001) planes (i.e., there are no hydrogen-bonding interactions parallel to the c-axis).[24] Why such a pattern of hydrogen bonding should be favored when the difference in size and/or charge of the M' and M'' ions increases is not clear.

When the size of the M' ion becomes sufficiently large octahedral coordination of the M' ion is no longer favored, and the $BaSn(OH)_6$-type structure appears. As discussed in the Results section this structure can be described as a CsCl-type packing of the Ba^{2+} and $[Sn(OH)_6]^{2-}$ ions, with the large Ba^{2+} ion sitting on an eight-coordinate site. A similar sort of transition is observed in the $M^{2+}SnF_6$ family. While $CaSnF_6$ and $SrSnF_6$ crystallize in an ReO_3-type structure with RS cation order and a six-coordinate site for the alkali metal cation, $BaSnF_6$ adopts a $KOsF_6$-type structure, where the Ba^{2+} ion is coordinated by 12 F^- ions.[25]

Finally we turn to the layered compounds like $LiSb(OH)_6$ and $CaPt(OH)_6$[26] that lie at the crossover from $a^+a^+a^+$ tilting to $a^+a^+c^-$ tilting in our structure map. As shown in Figure 8a,b,

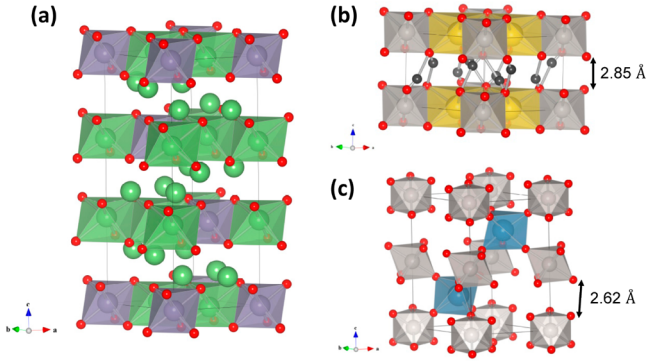

Figure 8. Crystal structures of (a) Li_8SnO_6 ($R\bar{3}$, a = 5.461 Å, c = 15.278 Å),[27] (b) $Na_2Pt(OD)_6$ ($P\bar{3}$, a = 5.831 Å, c = 4.755 Å),[28] and (c) $CaPt(OH)_6$ ($P\bar{3}1c$, a = 5.890 Å, c = 9.591 Å).[26] Li^+, Na^+, Ca^{2+}, Sn^{4+}, and Pt^{4+} are shown as green, yellow, blue, violet, and gray spheres, respectively. The O^{2-} and D^+ ions are shown as red and black spheres, respectively.

layered compounds such as Li_8SnO_6 and $Na_2Pt(OD)_6$ contain similar $M'_2M''O_6$ layers[27,28] as the $[Li_2Sb(OH)_6]^+$ layers found in $LiSb(OH)_6$. In $Na_2Pt(OD)_6$ oxygen atoms form a hexagonal closed-packed (hcp) sublattice, in which the octahedral void is occupied by either Na or Pt to form neutral $CdCl_2$-type layers.[28] The layers are interconnected via moderate strength hydrogen bonds ($D\cdots A$ distance: 2.85 Å).

The structure of $CaPt(OH)_6$, shown in Figure 8c, contains negatively charged $[Pt(OH)_6]^{2-}$ layers similar to the $[Sb(OH)_6]^-$ layers in $LiSb(OH)_6$. In $CaPt(OH)_6$ these layers are held together by ionic interactions with Ca^{2+} ions located between the layers.[26] Since Ca^{2+} and Na^+ have similar ionic radii (1.00 Å vs 1.02 Å for a six-coordinate ion)[19] one might wonder why Na^+ and Pt^{4+} form mixed layers in $Na_2Pt(OD)_6$, whereas Ca^{2+} and Pt^{4+} segregate into different layers in $CaPt(OH)_6$. The reason is likely due to differences in stoichiometry. In a mixed layer with a 2:1 ratio of the lower valent cation (e.g., Na^+) to the higher valent cation (e.g., Pt^{4+}), it is possible to adopt a pattern of ordering where octahedra containing the higher valent ion are isolated from each other. This is not possible in a $CdCl_2$-type layer with a 1:1 ratio of the two cations. A common theme in all of $M'M''(OH)_6$ structures is to keep the $[M''(OH)_6]^{n-}$ octahedra isolated from each other when the oxidation state of M'' is +4 or higher.

It is interesting that $LiSb(OH)_6$ does not adopt an ReO_3-type structure, in spite of the similar ionic sizes between Li^+ and

dx.doi.org/10.1021/ic5016252 | Inorg. Chem. 2014, 53, 10570−10577

Sb^{5+}, especially given the fact that related compounds $M'SbF_6$ (M′ = Li, Na) and $M'Sb(OH)_6$ (M′ = Na, Ag) do crystallize with an ordered ReO_3-type structure.[7,22] To explain this anomaly, we note the role of H^+ ion as a structural component in $LiSb(OH)_6$. For comparison, consider $CaSn(OH)_6$ or $NaSb(OH)_6$, where the cations are fairly large. The H^+ ion in such compounds is much smaller than the M′ cation, and hence can be structurally influential largely through hydrogen bonding. Conversely, in $LiSb(OH)_6$, the size of H^+ is not negligible compared with those of Sb^{5+} or Li^+, and one may consider the representation $(LiH_6)SbO_6$, where Li^+ and H^+ are treated as cations of similar radii. There exist many crystallographic similarities among $LiSb(OH)_6$ (Figure 4), Li_8SnO_6 (Figure 8a), and Li_7SbO_6 (not shown).[27,29] Apparently the combination of an hcp sublattice of oxide ions and small cations Li^+ and H^+ can provide a much denser packing than the ReO_3-type and is suitable for $LiSb(OH)_6$. After all it is well-known that the ReO_3-type structure can be regarded as perovskite with no dodecahedral ion whose ion packing is therefore relatively inefficient.

CONCLUSIONS

Colorless single crystals of $LiSb(OH)_6$, $SrSn(OH)_6$, and $BaSn(OH)_6$, have been synthesized by a low-temperature hydrothermal method using a Teflon-lined autoclave. The crystal structures were determined by single-crystal X-ray diffraction measurements. $LiSb(OH)_6$ takes a layered structure with the space group $P\bar{3}1m$, while $BaSn(OH)_6$ and $SrSn(OH)_6$ crystallize in a monoclinic structure with $P2_1/n$ symmetry. The latter structure contains a 3D $Sn(OH)_6$ framework and a distorted CsCl-type arrangement of Ba^{2+}/Sr^{2+} cations and $[Sn(OH)_6]^{2-}$ anions. The features and formation factors of these hitherto unknown crystal structures are discussed as part of a broader survey of hydroxides with $M(OH)_3$ or $M'M''(OH)_6$ stoichiometry. The relative sizes and electronegativities of the M′ and M″ ions play an important role in determining the most favorable structure type.

ASSOCIATED CONTENT

Supporting Information

Full crystallographic parameters for $BaSn(OH)_6$ and $SrSn(OH)_6$, thermogravimetric and differential thermal analysis plots, and X-ray powder diffraction data for $SrSn(OH)_6$. This material is available free of charge via the Internet at http://pubs.acs.org.

AUTHOR INFORMATION

Corresponding Author

*E-mail: woodward@chemistry.ohio-state.edu.

Notes

The authors declare no competing financial interest.

ACKNOWLEDGMENTS

We thank Dr. J. C. Gallucci, Dr. G. D. Renkes (The Ohio State University), Dr. Z. Tan, and Dr. K. Yamamoto (Osaka University) for experimental support. We are grateful to Dr. I. R. Evans (Durham University) for her single-crystal structure measurements and discussion.

REFERENCES

(1) (a) Guiffard, B.; Troccaz, M. *Mater. Res. Bull.* **1998**, *33*, 1759–1768. (b) Camargo, E. R.; Frantti, J.; Kakihana, M. *J. Mater. Chem.* **2001**, *11*, 1875–1879. (c) Li, F.; Liu, J.; Evans, D. G.; Duan, X. *Chem. Mater.* **2004**, *16*, 1597–1602. (d) Lou, X. W.; Deng, D.; Lee, J. Y.; Archer, L. A. *J. Mater. Chem.* **2008**, *18*, 4397–4401. (e) Bugaris, D. E.; Smith, M. D.; zur Loye, H.-C. *Inorg. Chem.* **2013**, *52*, 3836–3844. (f) Chance, M. W.; Bugaris, D. E.; Sefat, A. S.; zur Loye, H.-C. *Inorg. Chem.* **2013**, *52*, 11723–11733.

(2) (a) Wang, H. F.; Liu, Q. Z.; Chen, F.; Gao, G. Y.; Wu, W. *J. Appl. Phys.* **2007**, *101*, 106105/1–3. (b) Luo, X.; Oh, Y. S.; Sirenko, A.; Gao, P.; Tyson, T. A.; Char, K.; Cheong, S.-W. *Appl. Phys. Lett.* **2012**, *100*, 172112/1–5. (c) Kim, H.; Kim, U.; Kim, T.; Kim, J.; Kim, H.; Jeon, B.; Lee, W.; Mun, H.; Hong, K.; Yu, J.; Char, K.; Kim, K. *Phys. Rev. B* **2012**, *86*, 165205/1–9.

(3) (a) Mizoguchi, H.; Eng, H. W.; Woodward, P. M. *Inorg. Chem.* **2004**, *43*, 1667–1680. (b) Woodward, P. M.; Mizoguchi, H.; Kim, Y. I.; Stoltzfus, M. W. In *Metal Oxides;* Fierro, J. L. G., Ed.; Taylor & Francis: Boca Raton, FL, 2006; p 133. (c) Mizoguchi, H.; Chen, P.; Boolchand, P.; Ksenofontov, V.; Felser, C.; Barnes, P. W.; Woodward, P. M. *Chem. Mater.* **2013**, *25*, 3858–3866.

(4) Mizoguchi, H.; Woodward, P. M.; Park, C.-H.; Keszler, D. A. *J. Am. Chem. Soc.* **2004**, *126*, 9796–9800.

(5) (a) Hu, X.; Tang, Y.; Xiao, T.; Jiang, J.; Jia, Z.; Li, D.; Li, B.; Luo, L. *J. Phys. Chem. C* **2010**, *114*, 947–952. (b) Goto, K.; Nakachi, Y.; Ueda, K. *Thin Solid Films* **2008**, *516*, 5885–5889.

(6) (a) Buscaglia, M. T.; Leoni, M.; Viviani, M.; Buscaglia, V.; Martinelli, A.; Testino, A.; Nanni, P. *J. Mater. Res.* **2003**, *18*, 560–566. (b) Lu, W.; Schmidet, H. *J. Eur. Ceram. Soc.* **2005**, *25*, 919–925. (c) Chen, D.; Ye, J. *Chem. Mater.* **2007**, *19*, 4585–4591. (d) Kramer, J. W.; Isaacs, S. A.; Manivannan, V. *J. Mater. Sci.* **2009**, *44*, 3387–3392.

(7) Mitchell, R. H. *Perovskites Modern and Ancient;* Almaz, 2002.

(8) Wells, A. F. *Structural Inorganic Chemistry,* 5th Ed.; Clarendon: Wotton-under-Edge, 1984.

(9) (a) Chitrakar, R.; Abe, M. *Mater. Res. Bull.* **1988**, *23*, 1231–1240. (b) Yamamoto, O.; Li, S.; Sasamoto, T. *J. Mater. Synth. Process.* **1998**, *6*, 203–207.

(10) Schrewelius, N. *Z. Anorg. Allg. Chem.* **1938**, *238*, 241–254.

(11) Cheary, R. W.; Coelho, A. A. *J. Appl. Crystallogr.* **1992**, *25*, 109–121.

(12) *SMART Version 5.054 Data Collection and SAINT-Plus Version 6.45a Data Processing Software for the SMART System;* Bruker Analytical X-ray Instruments, Inc.: Madison, WI, 2003.

(13) Sheldrick, G. M. *SHELXTL Version 6.14;* Bruker Analytical X-ray Instruments, Inc.: Madison, WI, 2003.

(14) Brown, I. D. *J. Appl. Crystallogr.* **1996**, *29*, 479–480.

(15) Le Page, Y. *J. Appl. Crystallogr.* **1987**, *20*, 264–269.

(16) Mullica, D. F.; Beall, G. W.; Milligan, W. O.; Korp, J. D.; Bernal, I. *J. Inorg. Nucl. Chem.* **1979**, *41*, 277–282.

(17) (a) PDF00–056–0958; http://www.icdd.com/products/pdf2.htm (accessed March 2012). (b) PDF00–009–0086; http://www.icdd.com/index.htm (accessed March 2012).

(18) Basciano, L. C.; Peterson, R. T.; Roeder, P. L.; Swainson, I. *Can. Mineral.* **1998**, *36*, 1203–1210.

(19) Shannon, R. D. *Acta Crystallogr., Sect. A* **1976**, *32*, 751–767.

(20) Woodward, P. M. *Acta Crystallogr., Sect. B* **1997**, *53*, 44–66.

(21) Mizoguchi, H.; Woodward, P. M.; Byeon, S.-H.; Parise, J. B. *J. Am. Chem. Soc.* **2004**, *126*, 3175–3184.

(22) (a) Asai, A. *Bull. Chem. Soc. Jpn.* **1975**, *48*, 2677–2679. (b) Palenik, R. C.; Abboud, K. A.; Palenik, G. J. *Inorg. Chim. Acta* **2011**, *378*, 24–29.

(23) Lufaso, M. W.; Woodward, P. M. *Acta Crystallogr., Sect. B* **2001**, *57*, 725–738.

(24) Ross, N. L.; Chaplin, T. D.; Welch, M. D. *Am. Mineral.* **2002**, *87*, 1410–1414.

(25) (a) Mayer, H. W.; Reinen, D.; Heger, G. *J. Solid State Chem.* **1983**, *50*, 213–224. (b) Becker, S.; Benner, G.; Hoppe, R. *Z. Anorg. Allg. Chem.* **1990**, *591*, 7–16.

(26) Tremel, M.; Lupprich, E. *Z. Anorg. Allg. Chem.* **1975**, *414*, 169–175.

(27) Hoppe, R.; Braun, R. M. *Z. Anorg. Allg. Chem.* **1977**, *433*, 181–188.

(28) Bandel, G.; Mullner, M.; Tremel, M. *Z. Anorg. Allg. Chem.* **1979**, *453*, 5−8.
(29) Muhle, C.; Dinnebier, R. E.; v. Wullen, L.; Schwering, G.; Jansen, M. *Inorg. Chem.* **2004**, *43*, 874−881.